Bifurcation analysis of a semiconductor laser subject to non-instantaneous phase-conjugate feedback

Kirk Green

Department of Computer Science, K. U. Leuven, Celestijnenlaan 200A, 3001 Heverlee, Belgium

Bernd Krauskopf

Department of Engineering Mathematics, University of Bristol, Bristol BS8 1TR, UK

Abstract

We consider the question of how the behaviour of a semiconductor laser subject to phase-conjugate feedback depends on the interaction time of the phase-conjugating mirror. We employ continuation techniques to show how the bifurcation diagram in the plane of feedback strength versus pump current changes when the interaction time of the mirror is increased. This shows that for interaction times below 0.1 ns the assumption of instantaneous feedback is justified. On the other hand, increasingly larger interaction times lead to considerable changes in the locking region and a suppression of more complicated dynamics.

Key words: laser with phase-conjugate feedback, non-instantaneous feedback, delay differential equations, numerical continuation

The object of study of this paper is a semiconductor laser receiving phase-conjugate feedback (PCF) from a phase-conjugating mirror (PCM). An important physical difference compared to conventional optical feedback (COF) is that, for PCF, the laser light is wave-front inverted at the PCM. The return conjugated wave travels back along the exact path of the incident wave. Not only does this mean that the PCF laser is self-aligning, but also any distortions of the wave between the source and the PCM are undone on the return trip. This is of great physical value for high-resolution imaging techniques; the

Email addresses: kirk.green@cs.kuleuven.ac.be (Kirk Green), b.krauskopf@bristol.ac.uk (Bernd Krauskopf).

PCF laser has been shown to provide a great reduction in the linewidth [1,2], resulting in an extremely narrow and highly focused beam [3] which can be used for mode-locking and phase-locking [4].

The PCF laser is generally modelled by rate equations similar to those derived by Lang and Kobayashi [5], for the complex electric field E and the inversion N; these are introduced fully in Section 1. In this approach the feedback is modelled by a simple delay term involving the complex conjugate field after a fixed delay time τ. These equations have been used to study the dynamics and bifurcations of the PCF laser in considerable detail [6–10].

A main modelling assumption is that the PCM reacts instantaneously to the incident wave. However, in practice a PCM does not respond instantaneously because there is always some interaction time while the light passes through the PCM and the phase-conjugated wave is generated. The fastest PCF is from the response of a four-wave mixing (FWM) process in a Kerr-type nonlinear medium, such as a semiconductor material with counter-propagating pump beams. The interaction time is on the scale of femtoseconds to picoseconds in such devices [11]. However, particularly when the PCM is formed from a photo-reactive crystal or an atomic vapour [12] the interaction time can be much larger, on a nanosecond scale [13].

There is not much theoretical work to date on the effect of the interaction time with the PCM on the behaviour of the PCF laser. A model derived in Ref. [11] for non-instantaneous PCF takes the form of a delay differential equation (DDE) with a separate integral equation modelling the PCM with a finite interaction time; see Section 1 for the details. In Ref. [11] numerical simulation was used to show that, as the interaction time is increased, there is a suppression of chaotic dynamics for increasingly lower values of the feedback strength. Also investigated was the effect on the dynamics of varying the external-cavity length of the PCF laser. The influence of a finite reaction time on the stability region of the PCF laser was studied analytically in Refs. [14,15].

In this paper we consider the model of Ref. [11] and study the effect of the interaction time on the bifurcation diagram in the plane of feedback strength versus pump current. This work follows on from the bifurcation study near the locking region in Ref. [10] for the case of instantaneous PCF. Specifically, we show how the locking range of the PCF laser changes with increasing interaction time. For very small interaction times, as can be achieved by using semiconductor lasers to produce PCF, the assumption of instantaneous feedback appears to be justified. However, for larger interaction times we find that regions bounded by Hopf bifurcations start to interact with one another, leading to dramatic changes in the shape of the locking range of the PCF laser. This allows us to present a more global view of the suppression of complicated dynamics reported in Ref. [11].

In our study we make use of advanced numerical tools for DDEs, namely the continuation package DDE-BIFTOOL [16]. This software goes much beyond numerical simulation of the governing equations and allows one to numerically find and follow steady states and periodic orbits irrespective of their stability. Furthermore, certain bifurcations can be detected and followed in parameters. The study of semiconductor lasers subject to optical feedback [17–19] has emerged as arguably the biggest area of application of numerical continuation. Recent work includes that on edge emitting lasers with COF in Refs. [20–22] and a vertical-cavity surface emitting laser with COF in Ref. [23], and our work on the PCF laser in Refs. [7–10].

This paper is organised as follows. In Section 1 we introduce the rate equations for non-instantaneous PCF and show simulations illustrating the suppression of complicated dynamics. In Section 2 we present bifurcation diagrams obtained by continuation. Specifically, in Section 2.1 we study the bifurcations involved in the locking mechanisms of the PCF laser in the plane of feedback strength versus pump current as the interaction time is varied. In Section 2.2 we consider a larger region of the parameter plane in order to compare with the results obtained by simulation. Finally in Section 3 we draw conclusions and discuss future work.

1 Rate equations for non-instantaneous PCF

A single-mode semiconductor laser subject to weak PCF can be described by the following rate equations

$$\frac{dE}{dt} = \frac{1}{2}\left[-i\alpha G_N(N(t) - N_{\text{sol}}) + \left(G(t) - \frac{1}{\tau_p}\right)\right] E(t) + \kappa F(t,\tau), \tag{1}$$

$$\frac{dN}{dt} = \frac{I}{q} - \frac{N(t)}{\tau_e} - G(t)\,|E(t)|^2 \tag{2}$$

for the evolution of the slowly varying complex electric field $E(t)$ and the population inversion $N(t)$. Nonlinear gain is included as $G(t) = G_N(N(t) - N_0(1 - \epsilon P(t))$, where $\epsilon = 3.57 \times 10^{-8}$ is the nonlinear gain coefficient and $P(t) = |E(t)|^2$ is the intensity. Furthermore, $N_{\text{sol}} = N_0 + 1/(G_N\tau_p)$. Parameter values correspond to a Ga-Al-As semiconductor laser, namely: the linewidth enhancement factor $\alpha = 3$; the optical gain $G_N = 1190\,\text{s}^{-1}$; the photon lifetime $\tau_p = 1.4\,\text{ps}$; the electron charge $q = 1.6 \times 10^{-19}\,\text{C}$; the electron lifetime $\tau_e = 2\,\text{ns}$; and the transparency electron number $N_0 = 1.64 \times 10^8$.

The feedback term $\kappa F(t,\tau)$ in Eq. (1) involves the feedback rate κ and the external-cavity round-trip time τ. They are given by

$$\kappa = \frac{(1-R_m)}{\tau_L}\left[\frac{R_{\rm ext}}{R_m}\right]^{1/2} \quad \text{and} \quad \tau = \frac{2L_{\rm ext}}{c},$$

where $R_m = 0.12$ is the laser front-facet reflectivity, $\tau_L = 9.3\,\text{ps}$ is the round-trip time in the solitary laser cavity, $R_{\rm ext}$ is the power reflectivity of the PCM, $L_{\rm ext}$ is the length of the external-cavity, and c is the velocity of light. We fix τ at the realistic value of $\tau = 2/3\,\text{ns}$, corresponding to $L_{\rm ext} \approx 10\,\text{cm}$. In the simulation below we fix the value of the pump current to $I = 65.1$ mA and consider the dynamics as a function of the dimensionless bifurcation parameter $\kappa\tau$. In the two-parameter continuation studies we also free the pump current parameter I. Note that both $\kappa\tau$ and I are experimentally accessible parameters.

For the case of an instantaneously responding PCM, the PCF function in Eq. (1) reduces to $F(t,\tau) = E^*(t-\tau)$; see Refs. [6–10,24]. An improved PCF model is derived in Ref. [11] where a single-Lorentzian approximation for non-instantaneous feedback is given as

$$F(t,\tau) = \frac{1}{t_m}\exp\left[-2i\delta_0(t-\tau/2)\right] \cdot \int_{-\infty}^{t} E^*(t'-\tau)\exp\left[-\frac{(1-i\delta_0 t_m)(t-t')}{t_m}\right]dt'\,.$$

In Ref. [11] the authors used a recurrence relation to solve this integral equation. Here we differentiate with respect to time to obtain the differential equation

$$\frac{dF}{dt} = \frac{1}{t_m}\left(E^*(t-\tau)\exp\left[-2i\delta_0(t-\tau/2)\right] - (1-i\delta_0 t_m)F(t)\right) \tag{3}$$

for the complex feedback field $F(t)$. Here the interaction time t_m is related to the effective depth or length of the PCM [11]. The parameter δ_0 corresponds to a detuning from the pump laser used for FWM. As is common in the field, we set $\delta_0 = 0$. For studies of how variations in δ_0 affect the dynamics of the PCF laser see Refs. [14,15]. Note that in Eq. (3) as $t_m \to 0$ we recover the equation for instantaneous PCF because $F(t,\tau) \to E^*(t-\tau)$.

Thus the semiconductor laser subject to PCF from a finite penetration PCM is described by Eqs. (1)–(3). These equations have $\mathbb{Z}_2$-symmetry under the transformation $(E,F,N) \to (-E,-F,N)$, where the symmetry group is $\mathbb{Z}_2 = \{1,-1\}$, corresponding to rotations over π of the complex E and F planes. Physically, this corresponds to a phase shift by π of the electric field.

To relate to the previous work in Ref. [11] we show in Fig. 1 the attracting dynamics as found by numerical simulation of Eqs. (1)–(3) for the fixed value of

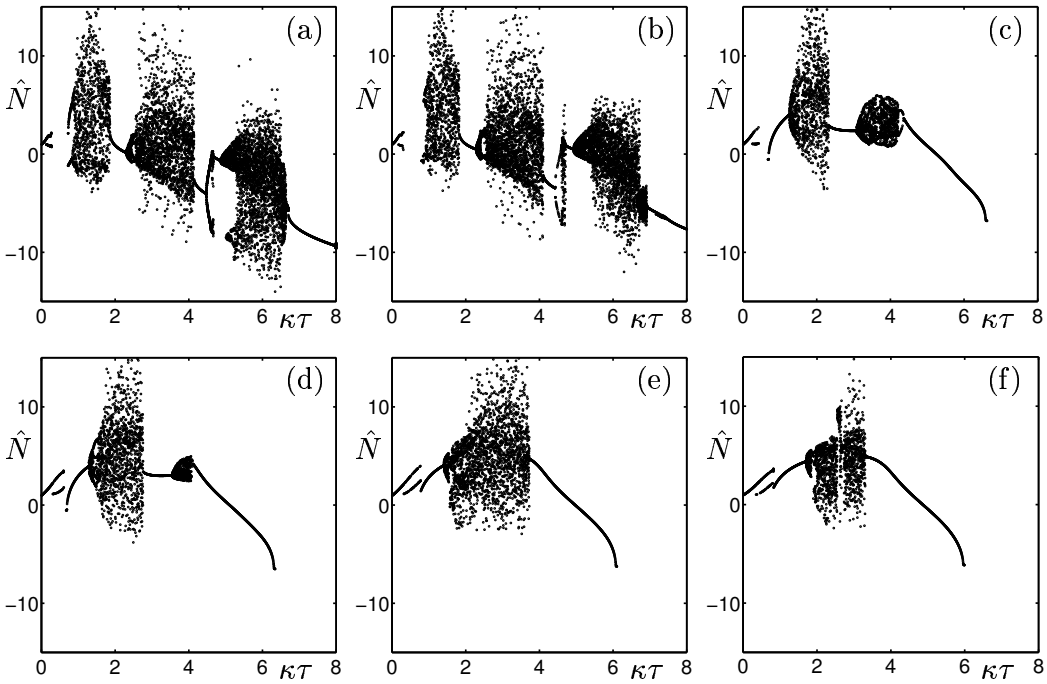

Fig. 1. Bifurcation diagrams obtained by simulation for $I = 65.1$ mA. From (a) to (f) t_m takes the values 0.0 ns, 0.05 ns, 0.28 ns, 0.4 ns, 0.64 ns, and 1.0 ns.

the pump current $I = 65.1$ mA and increasing interaction time t_m. Specifically, after transients died away, for each value of $\kappa\tau$ a normalised value of inversion $\hat{N} = (N/N_{\text{sol}} - 1) \times 10^3$ was plotted whenever the intensity $P(t) = |E(t)|^2$ crossed its average value in the positive direction. For a single value of $\kappa\tau$, an absence of points corresponds to a steady state, locked solution, a small number of points correspond to a periodic solution, and a large number of points correspond to quasiperiodic or chaotic dynamics.

Figure 1 (a) shows the case of instantaneous PCF; that is $t_m = 0$ ns. One sees the typical picture of stable periodic laser output (also called external cavity modes [7]) with 'bubbles' of chaos between them; see also Refs. [6–10,24]. It has been shown that the periodic solutions are interconnected via an unstable steady state solution [7]. The region where the steady state solution is stable is called the *locking region* of the PCF laser [10]; it is identified by an absence of points in Fig. 1 (a). Physically, locking corresponds to a frequency match between the solitary laser and the pump lasers used in the FWM process to form the PCM [18]. This frequency-locked and phased-locked solution has been shown to produce an extremely narrow linewidth which is stable even with the addition of noise [25]. This is a main reason why PCF has been of great interest to physical application.

Figures 1 (b) to (f) show how the attracting dynamics change for increasing values of the interaction time t_m. For the small interaction time of $t_m = 0.05$ ns in Fig. 1 (b) there is little qualitative difference with the case of $t_m = 0$ ns.

This demonstrates that the assumption in previous studies of instantaneous PCF is justified for sufficiently fast PCMs. However, as t_m is increased further, the dynamical picture within our $\kappa\tau$-range of consideration changes. Figure 1 (c), for $t_m = 0.28$ ns, reveals that the second bubble of chaos has diminished in size, while the third bubble of chaos has disappeared completely. Note that the periodic solution emanating from the second bubble is shown to bifurcate at $\kappa\tau \approx 6.60$ to a steady state solution. In other words, we observe a second region of locking for higher values of feedback!

As shown in Fig. 1 (d), for $t_m = 0.4$ ns the second bubble of chaos is replaced by a quasiperiodic attractor. The periodic solution is again shown to bifurcate to a locked solution at $\kappa\tau \approx 6.32$. As t_m is increased further, the second bubble disappears altogether; see Fig. 1 (e) for $t_m = 0.64$ ns. The range of the periodic solution emanating from the first and only bubble of chaos has increased and bifurcates to a locked, steady state solution at $\kappa\tau \approx 6.08$. This is also the dynamical picture for $t_m = 1.0$ ns, that is, we observe a single bubble of chaos; see Fig. 1 (f). This suppression of chaotic dynamics was first observed in Ref. [11].

2 Bifurcation diagrams obtained by continuation

The one-parameter bifurcation diagrams shown in Fig. 1 provide us with insight into what is happening to the stable, attracting solutions of the PCF laser. However, they do not explain why the bubbles of chaos are suppressed, or give any insight into the bifurcations bounding the locking region. For this we need to turn to continuation techniques.

The bifurcation diagrams of Figs. 2, 3 and 4 were obtained with the continuation package DDE-BIFTOOL [16]. Roughly speaking, DDE-BIFTOOL has the same functionality as early versions of continuation software for ordinary differential equations, for example, AUTO [26] and HomCont [27]. Steady states and periodic solutions can be followed in one parameter and bifurcation points noted. Bifurcations of steady states and connecting orbits [28] can be followed in two or more parameters. In Ref. [10], continuation techniques were used to detect and follow, in two parameters, the bifurcations involved in the locking mechanism of the PCF laser. Bifurcations of steady states observed included saddle-node bifurcations and pitch-fork bifurcations, both of which correspond to a real eigenvalue at $+1$, Hopf bifurcations corresponding to a pair of purely imaginary complex conjugate eigenvalues, and a heteroclinic connection between two non-symmetric saddle steady states. Furthermore, a number of codimension-two bifurcations were found, including a double-Hopf point and a T-point bifurcation of heteroclinic orbits. For more details of these bifurcations see, for example, Ref. [29].

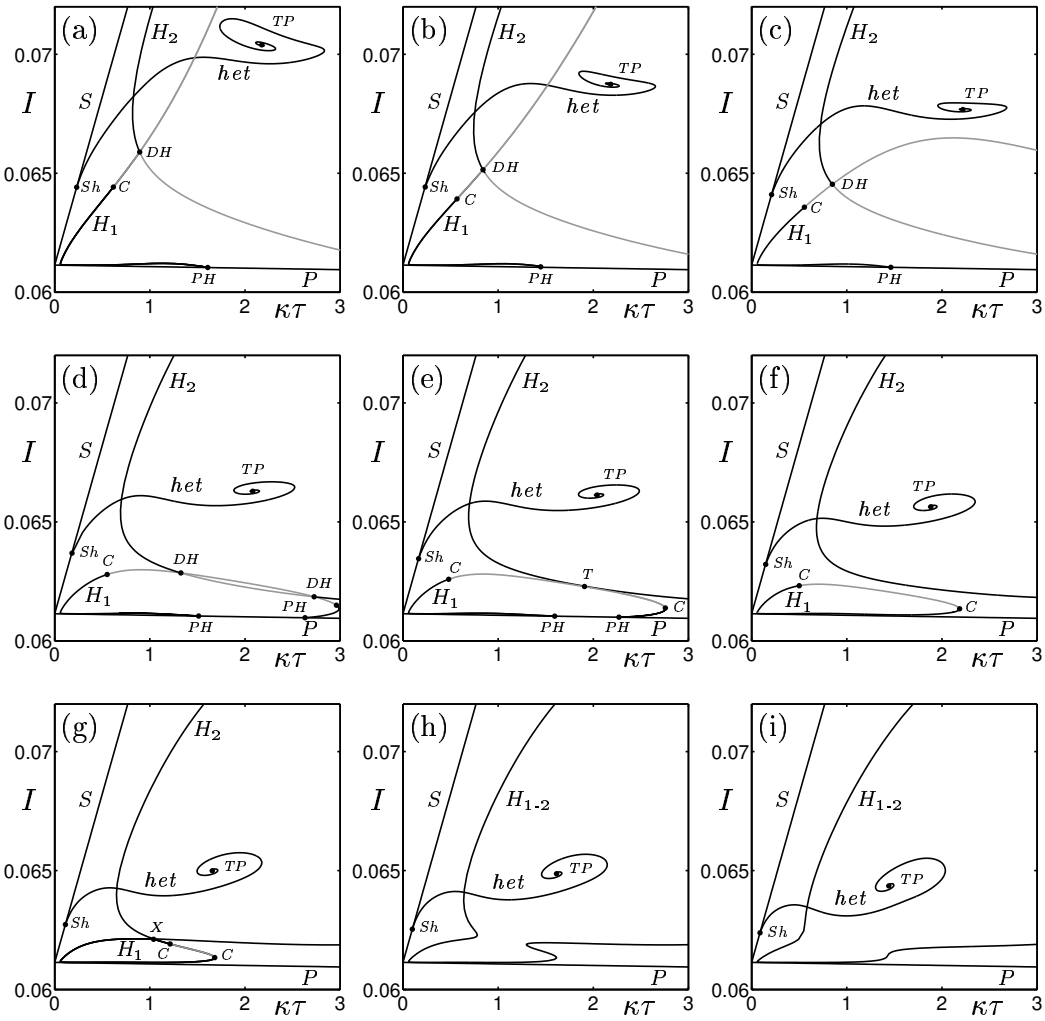

Fig. 2. Bifurcation diagram in the $(\kappa\tau, I)$-plane near the locking region of the PCF laser. From (a) to (i) t_m takes the values 0.0 ns, 0.05 ns, 0.1 ns, 0.25 ns, 0.28 ns, 0.4 ns, 0.64 ns, 0.7 ns, and 1.0 ns.

In Section 2.1, we show what effect the PCM interaction time t_m has on the bifurcations bounding the locking region. We increase our parameter range of interest in Section 2.2 where we consider what effect the interaction time has over the entire $\kappa\tau$-range that was considered by simulation in Section 1 and in Refs. [6,11,24].

2.1 The locking region

Figure 2 shows bifurcation diagrams obtained by continuation with DDE-BIFTOOL. Plotted are straight lines of saddle-node bifurcations S and pitchfork bifurcations P. Curves of Hopf bifurcations H_i are drawn dark when the Hopf bifurcation is supercritical, that is, when the bifurcating periodic solu-

tion is stable, and lighter when it is subcritical and the bifurcating periodic solution is unstable. Changes in criticality of Hopf bifurcations are marked by a point *C*. Double-Hopf points *DH* are shown where two Hopf curves cross. Also shown is a curve of heteroclinic orbits *het*. This curve is born in a saddle-node heteroclinic bifurcation *Sh*. In Ref. [10] this curve was shown to end in a codimension-two bifurcation point *TP* of heteroclinics orbits known as a T-point [30]. Here we show that this codimension-two bifurcation persists as the interaction time is increased.

We begin our discussion with the case of instantaneous feedback $t_m = 0$ ns shown in Fig. 2 (a), which is as presented in Ref. [10]. Below the curve P the off-state of the PCF laser is stable, and above P it is unstable. In other words, physically P is the threshold curve [10]. The locking region is the region bounded to the left by a curve of saddle-node bifurcations S and to the right by curves of Hopf bifurcations H_1 and H_2. At S two stable non-symmetric locked steady state solutions and two unstable non-symmetric saddle steady states are born. At H_1 and H_2 the locked solution is destabilised and a periodic solution is born.

The curve *het* is of heteroclinic connections between the two non-symmetric saddle steady states born at the curve *S*. At the curve *het*, a symmetric periodic solution born at the onset of feedback $\kappa\tau$ simultaneously hits the two non-symmetric saddle steady states. This results in two non-symmetric heteroclinic orbits [8]. The curve *het* is seen to cross the locking region. Above the curve *het*, but between the curves S and H_2, we observe a bistability between the periodic solution born at the onset of feedback $\kappa\tau$ and the stable steady state solution born at the curve *S*. A second bistability exists above the curve *het* and to the right of the Hopf curve H_2. Here the bistability is between the stable periodic solution emanating from the Hopf bifurcation H_2 and the periodic solution born at the onset of feedback $\kappa\tau$.

Other features in Fig. 2 (a) include a codimension-two double-Hopf point *DH* where the Hopf curves H_1 and H_2 intersect, a saddle-node heteroclinic point *Sh* where the curves S and *het* meet, and a pitchfork-Hopf point *PH* where the curves P and H_1 meet. Furthermore, the curve *het* is shown to end in a spiral. This marks a codimension-two bifurcation of the heteroclinic orbit, known as a T-point bifurcation *TP*. At the point *TP*, the heteroclinic orbit collides with the trivial steady state solution; that is $(E, N) = (0, I/q)$, resulting in two bifurcating heteroclinic orbits; see Ref. [10]. Physically, heteroclinic orbits are important because near such special solutions the laser is generally *excitable* [31].

Figures 2 (b) and (c) show that, as the interaction time is increased to $t_m = 0.05$ ns and $t_m = 0.1$ ns, respectively, the dynamical picture of the locking range does not change much compared with the instantaneous feedback case

in Fig. 2 (a). The only noticeable differences are that in Fig. 2 (c) the curve H_2 drops below the T-point *TP* and the curve *het* crosses the locking region at slightly lower values of pump current I.

However, for $t_m = 0.25$ ns, the curve H_2 is seen to cross the curve H_1 at two double-Hopf points *DH*; see Fig. 2 (d). For $t_m = 0.28$ ns, Fig. 2 (e) reveals that the curves H_1 and H_2 meet at a tangency T. This marks the disappearance of the double-Hopf point *DH*. Also, for low values of I and high values of $\kappa\tau$, the laser is shown to lock again. Figure 2 (f), for $t_m = 0.4$ ns, shows that the curve H_1 eventually forms a single closed loop, having 'lifted' off the pitchfork curve P. Furthermore, this loop is isolated, meaning that it is separated from the curve H_2 by a region of locking. In other words, the locking region for large values and that for low values of $\kappa\tau$ are now joined between H_1 and H_2. Notice that for $I = 65.1$ mA the curve *het* is very close to the curve H_2. This explains why we observed in the simulation for low values of feedback that the periodic solutions at either side of the locking region came together; see Fig. 1 (e). While the length of the locking region does not diminish, the periodic solution born at the onset of feedback is destabilised at the curve *het* for higher values of $\kappa\tau$.

As t_m is increased further, Fig. 2 (g), for $t_m = 0.64$ ns, shows that the curves H_1 and H_2 meet again. However, this time, not at a tangency but at a singularity point X. (This is a classic singularity, namely a saddle of the two-dimensional surface of Hopf bifurcations in the three-dimensional $(\kappa\tau, I, t_m)$-space; see, for example, Ref. [32].) After the singularity the curves H_1 and H_2 connect locally in a different way, so that they coalesce to form a single curve of Hopf bifurcations $H_{1\text{-}2}$; see Figs. 2 (h) and (i). Note that throughout this entire bifurcation scenario, the T-point bifurcation was shown to persist.

2.2 The larger picture

In this section, in order to further compare continuation results with those shown by simulation in Fig. 1, we extend the area of the $(\kappa\tau, I)$-plane under consideration to $[0, 8] \times [0.057, 0.1]$. Bifurcation points are marked as in Fig. 2. Once again, Figs. 3 (a), (b) and (c) show that the scenarios for instantaneous feedback $t_m = 0$ ns and finite interaction times of $t_m = 0.01$ ns and $t_m = 0.05$ ns, respectively, are very similar. The main difference being that, for $t_m = 0.05$ ns, we observe an upper turning point (a maximum) of the Hopf curve H_1 in our region of interest. In Fig. 3 (d), for $t_m = 0.1$ ns, the curve H_1 is shown to begin and end at the pitchfork curve P, at a pitchfork Hopf bifurcation points *PH*. We also observe a maximum in the Hopf curve H_2. In Fig. 3 (e), for $t_m = 0.15$ ns, the curve H_2 is shown to close, although at this stage it still overlaps the curves H_1 and H_3. This has the implication that for high feedback

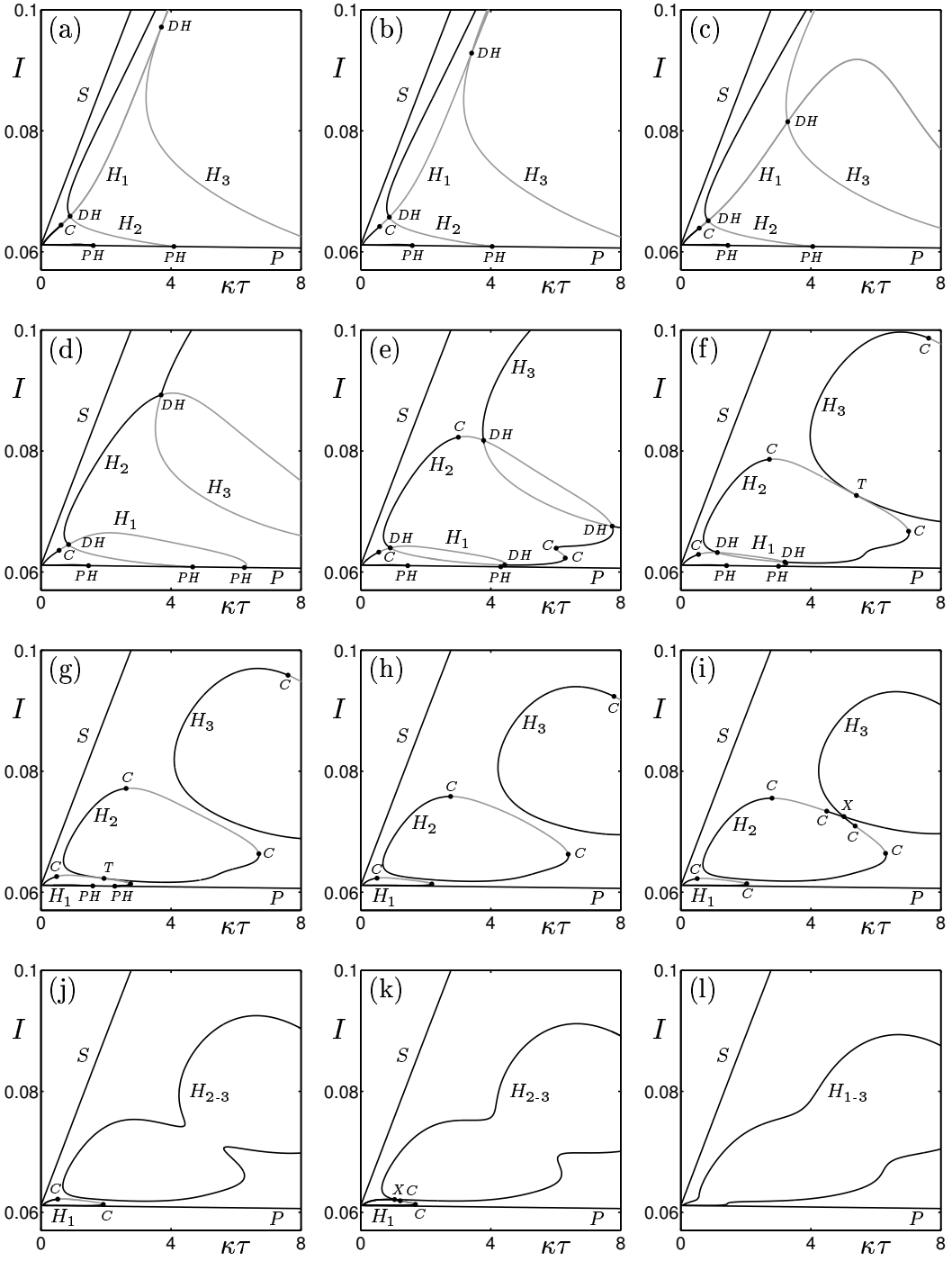

Fig. 3. Bifurcation diagram in the $(\kappa\tau, I)$-plane. From (a) to (l) t_m takes the values 0.0 ns, 0.01 ns, 0.05 ns, 0.1 ns, 0.15 ns, 0.28 ns, 0.4 ns, 0.452 ns, 0.5 ns, 0.64 ns, and 1.0 ns.

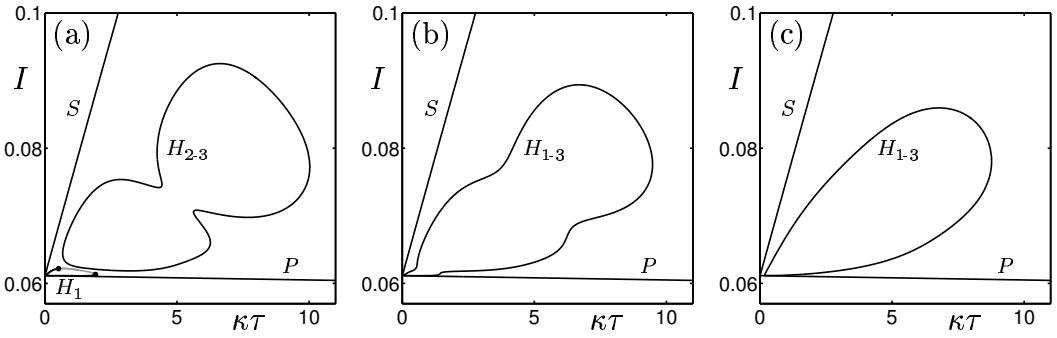

Fig. 4. Bifurcation diagram in the $(\kappa\tau, I)$-plane. From (a) to (c) t_m takes the values 0.5 ns, 1.0 ns, and 10.0 ns.

and low pump current the laser is shown to lock again; see the lower right of Fig. 3 (e).

In Fig. 3 (f), for $t_m = 0.22$ ns, the Hopf curves H_2 and H_3 form a tangency T, after which they separate. This is shown in Fig. 3 (g), where for $t_m = 0.28$ ns the curves H_1 and H_2 now form a tangency T; compare with Fig. 2 (e). As t_m is increased, the curves H_1, H_2 and H_3 are all isolated (that is, do not intersect each other). In fact, Fig. 3 (h), for $t_m = 0.4$ ns, shows that the curve H_1 has 'lifted' off the pitchfork curve P resulting in three isolated regions bounded by Hopf bifurcations; compare with Fig. 2 (f). As t_m is increased the curve of Hopf bifurcations H_2 again meets the curve H_3, but this time at a singularity point X; see Fig. 3 (i), for $t_m = 0.452$ ns. After the singularity X, Fig. 3 (j), for $t_m = 0.5$ ns, the curves H_2 and H_3 have coalesced to form a single curve $H_{2\text{-}3}$. For $t_m = 0.64$ ns, this single curve $H_{2\text{-}3}$ is shown to form a further singularity X with the curve H_1; see Fig. 3 (k) and also Fig. 1 (f). After this second singularity all three Hopf curves form a single curve. This is shown in Fig. 3 (l), where for $t_m = 1.0$ ns we see a single curve of Hopf bifurcations $H_{1\text{-}3}$.

In Fig. 4 we increase the size of the $(\kappa\tau, I)$-plane to $[0, 11] \times [0.057, 0.1]$ to highlight the bifurcations that lead to the single curve $H_{1\text{-}3}$. Fig. 4 (a), for $t_m = 0.5$ ns, shows the closed Hopf curve $H_{2\text{-}3}$; compare with Fig. 3 (j). As t_m is increased, the curve H_1 coalesces with $H_{2\text{-}3}$ to form the single closed curve $H_{1\text{-}3}$ shown in Fig. 4 (b) for $t_m = 1.0$ ns; compare with Fig. 3 (k). The curve $H_{1\text{-}3}$ persists for even higher values of t_m. Figure 4 (c), for $t_m = 10.0$ ns, shows that $H_{1\text{-}3}$ eventually develops the form a single drop-like, convex curve. Physically, such a high value of t_m corresponds to the interaction time of a PCM formed by an atomic vapour.

The isolated regions bounded by supercritical Hopf bifurcations coincide with the suppression of chaotic bubbles we observed in Fig. 1 and reported in Ref. [11]. This is of no surprise because, as can be seen in Fig. 1, the complex dynamics originate from bifurcations of the periodic solutions born in the Hopf bifurcations. Therefore, one would expect these complex, chaotic dynamics to be confined within these isolated regions bounded by Hopf bifurcations.

3 Conclusions

We have investigated the effect of the interaction time of a finite-depth PCM. As the interaction time was increased, simulations show that regions of chaotic output are suppressed. It was also revealed that the PCF laser locks again for higher values of feedback.

Using continuation techniques, we presented a sequence of two-parameter bifurcations diagrams near the locking region of the PCF laser. This revealed that the bifurcation scenario for an instantaneous PCM presented in Ref. [10] is robust up to an interaction time of the PCM of about 0.1 ns. Individual features of the bifurcation diagram, in particular a curve of heteroclinic orbits ending in a T-point bifurcation, persist as the interaction time was increased further. On the other hand, for larger interaction times we found a scenario that changed the bifurcation diagram near the locking region and beyond. Specifically, we found that curves of Hopf bifurcations may bound isolated regions which decreased in size as the interaction time was increased. The periodic solutions born in these Hopf bifurcations are those that undergo the further bifurcations to chaos that were observed by simulation. Therefore, we identify the suppression of the chaotic dynamics with the changes in the regions bounded by Hopf bifurcations.

At present it is not possible to follow these further bifurcations of the periodic solutions in two parameters. When the necessary continuation techniques become available, even greater light can be shed on how the transitions to chaos in the PCF laser depend on the interaction time of the PCM.

We finally remark that some PCMs, such as atomic vapour cells [13], have a limited bandwidth of the conjugated light. This realisation was one motivation for the recent interest in filtered optical feedback (FOF) [33]. We remark that the equations describing the FOF laser are very similar to those for the non-instantaneous PCF laser discussed here. A further investigation of the similarities and differences between these two delay systems is an interesting topic for future research.

Acknowledgements

The authors thank Tom Gavrielides and Giovanni Samaey for helpful discussions. K.G. is a Research Fellow of K. U. Leuven (Belgium). The research of B.K. was supported by an EPSRC Advanced Research Fellowship grant.

References

[1] P. Kurz, T. Mukai, Frequency stabilization of a semiconductor laser by external phase conjugate feedback, Opt. Lett. 21 (1996) 1369–1371.

[2] M. Ohstu, I. Koshiishi, Y. Teramachi, A semiconductor laser as a stable phase conjugate mirror for linewidth reduction of another semiconductor laser, Jpn. J. Appl. Phys. 29 (1990) 2060–2062.

[3] C. R. Giuliano, Applications of optical phase conjugation, Physics Today 34(4) (1981) 27–35.

[4] G. R. Gray, D. H. DeTienne, G. P. Agrawal, Mode locking in semiconductor lasers by phase-conjugate optical feedback, Opt. Lett. 20 (1995) 1295–1297.

[5] R. Lang, K. Kobayashi, External optical feedback effects on semiconductor injection laser properties, IEEE J. Quantum Electron. 16(3) (1980) 347–355.

[6] B. Krauskopf, G. R. Gray, D. Lenstra, Semiconductor laser with phase-conjugate feedback: Dynamics and bifurcations, Phys. Rev. E 58 (1998) 7190–7196.

[7] K. Green, B. Krauskopf, Bifurcation analysis of frequency locking in a semiconductor laser with phase-conjugate feedback, Int. J. Bif. Chaos 13(9) (2003); to appear. (`http://www.enm.bris.ac.uk/anm/preprints/2002r06.html`)

[8] K. Green, B. Krauskopf, Global bifurcations and bistability at the locking boundaries of a semiconductor laser with phase-conjugate feedback, Phys. Rev. E 66 (2002) 016220.

[9] K. Green, B. Krauskopf, K. Engelborghs, Bistability and torus break-up in a semiconductor laser with phase-conjugate feedback, Physica D 173(2002) 114–129.

[10] K. Green, B. Krauskopf, G. Samaey, A two-parameter study of the locking region of a semiconductor laser subject to phase-conjugate feedback, SIAM J. Dynam. Syst. 2(2) (2003) 254–276.

[11] D. H. DeTienne, G. R. Gray, G. P. Agrawal, D. Lenstra, Semiconductor laser dynamics for feedback from a finite-penetration-depth phase-conjugate mirror, IEEE J. Quantum Electron. 33 (1997) 838–844.

[12] N. Cyr, C. N. Breton, M. Tetu, S. Theriault, Laser-diode frequency control by resonant phase-conjugate reflection from an atomic vapor, Opt. Lett. 16 (1991) 1298–1300.

[13] O. K. Anderson, A. P. A. Fischer, I. C. Lane, E. Louvergneaux, S. Stolte, D. Lenstra, Experimental stability diagram of a diode laser subject to weak phase-conjugate feedback from a rubidium vapor cell, IEEE J. Quantum Electron. 35 (1999) 577–582.

[14] W. A. van der Graaf, L. Pesquera, D. Lenstra, Stability of a diode laser with phase-conjugate feedback, Opt. Lett. 23(4) (1998) 256–258.

[15] W. A. van der Graaf, L. Pesquera, D. Lenstra, Stability and noise properties of diode lasers with phase-conjugate feedback, IEEE J. Quantum Electron., 37(4) (2001) 562–573.

[16] K. Engelborghs, T. Luzyanina, G. Samaey, DDE-BIFTOOL v2.00: a Matlab package for bifurcation analysis of delay differential equations, Technical Report TW-330, Department of Computer Science, K. U. Leuven, Belgium, 2001. (`http://www.cs.kuleuven.ac.be/~koen/delay/ddebiftool.shtml`)

[17] B. Krauskopf, D. Lenstra, editors. Fundamental Issues of Nonlinear Laser Dynamics, volume 548. AIP Conf. Proc., 2000.

[18] G. H. M. Van Tartwijk, G. P. Agrawal, Laser instabilities: a modern perspective. Prog. Quantum Electron. 22 (1998) 43–122.

[19] G. H. M. Van Tartwijk, D. Lenstra, Semiconductor lasers with optical injection and feedback, Quantum Semiclass. Opt., 7 (1995) 87–143.

[20] B. Haegeman, K. Engelborghs, D. Roose, D. Pieroux, T. Erneux, Stability and rupture of bifurcation bridges in semiconductor lasers subject to optical feedback, Phys. Rev. E 66 (2002) 046216.

[21] D. Pieroux, T. Erneux, B. Haegeman, K. Engelborghs, D. Roose, Bridges of periodic solutions and tori in semiconductor lasers subject to delay, Phys. Rev. Lett. 87 (2001) 193901.

[22] D. Pieroux, T. Erneux, T. Luzyanina, K. Engelborghs, Interacting pairs of periodic solutions lead to tori in lasers subject to delayed feedback, Phys. Rev. E 63 (2001) 036211.

[23] M. Sciamanna, T. Erneux, F. Rogister, O. Deparis, P. Megret, M. Blondel, Bifurcation bridges between external-cavity modes lead to polarization self-modulation in vertical-cavity surface-emitting lasers, Phys. Rev. A 65 (2002) 041801(R).

[24] G. R. Gray, D. Huang, G. P. Agrawal, Chaotic dynamics of semiconductor lasers with phase-conjugate feedback, Phys. Rev. A 49 (1994) 2096–2105.

[25] G. P. Agrawal, G. R. Gray, Effect of phase-conjugate feedback on the noise characteristics of semiconductor lasers, Phys. Rev. A 46 (1992) 5890–5898.

[26] E. Doedel, A. R. Champneys, T. Fairgrieve, Yu. Kuznetsov, B. Sandstede, X. Wang, AUTO 97: Continuation and bifurcation software for ordinary differential equations, 1997. (`http://indy.cs.concordia.ca/auto/main.html`)

[27] A. R. Champneys, Y. A. Kuznetsov, B. Sandstede. A numerical toolbox for homoclinic bifurcation analysis. Int. J. Bif. Chaos, 6(5) (1996) 867–887.

[28] G. Samaey, K. Engelborghs, D. Roose, Computation of connecting orbits in delay differential equations, Numer. Algorithms 30 (2002) 335–352.

[29] Y. Kuznetsov, Elements of Applied Bifurcation Theory, Springer, Berlin, 1995.

[30] P. Glendinning, C. Sparrow, T-points: A codimension two heteroclinic bifurcation, Journal of Statist. Phys. 43 (1986) 479–488.

[31] B. Krauskopf, K. R. Schneider, J. Sieber, S. M. Wieczorek, M. Wolfrum, Excitability and self-pulsations near homoclinic bifurcations in semiconductor laser systems, Opt. Commun. 215(4-6) (2003) 367–379.

[32] V. I. Arnol'd, Catastrophe Theory, 3rd edition. Springer, Berlin, 1992.

[33] M. Yousefi, D. Lenstra, G. Vemuri, Nonlinear dynamics of a semiconductor laser with filtered optical feedback and the influence of noise, Phys. Rev. E, 67 (2003) 046213.